Journal of Nuclear Materials 526 (2019) 151771

Contents lists available at ScienceDirect

Journal of Nuclear Materials

journal homepage: www.elsevier.com/locate/jnucmat

Investigation of the thermal and neutron irradiation response of BAM-11 bulk metallic glass

J. Brechtl [a, b, *], H. Wang [a], N.A.P.K. Kumar [b], T. Yang [a], Y.-R. Lin [a], H. Bei [b], J. Neuefeind [b], W. Dmowski [b], S.J. Zinkle [a, b, **]

[a] University of Tennessee, Knoxville, TN, 37996, USA
[b] Oak Ridge National Laboratory, Oak Ridge, TN, 37831, USA

ARTICLE INFO

Article history:
Received 16 July 2019
Received in revised form
24 August 2019
Accepted 26 August 2019
Available online 29 August 2019

Keywords:
Metallic glasses
Irradiation effects
Annealing
Microstructure
Nanoindentation
Neutron diffraction

ABSTRACT

$Zr_{52.5}Cu_{17.9}Ni_{14.6}Al_{10}Ti_5$ (BAM-11) bulk metallic glass was irradiated by neutrons to a fluence of 1.4×10^{20} n/cm^2 (E > 0.1 MeV) (0.1 displacements per atom, dpa) at a temperature of ~70 °C and then analyzed using multiple mechanical property and structural characterization techniques. Nanoindentation hardness measurements revealed that irradiation led to softening and a reduced Young's modulus in the alloy while annealing at 300–325 °C caused an increase in the hardness and modulus. Neutron diffraction results indicated that primary knock-on events caused rejuvenation (structural disordering) while annealing resulted in structural relaxation. Furthermore, it was found that annealing after irradiation reversed the disordering effects caused by the irradiation. The increased disordering in the alloy during irradiation is thought to be attributed to the enhanced free volume content caused by the neutron collision cascades in the matrix. Indeed, immersion density measurements revealed that irradiation led to a decrease in the density of the alloy. This decrease in the macroscopic density was linked to an increase in the structural disorder of the alloy while an increase in the density corresponded to an increasing degree of order. Additionally, synchrotron X-ray diffraction related the structural relaxation of the alloy to a loss of ductility, which is in agreement with the literature. Overall, an increase in the structural disorder in the sample is linked to a softening of the alloy and to a higher concentration of soft-zone defects in the glass.

1. Introduction

Bulk metallic glasses (BMGs), are composed of a disordered structure which prohibits the creation of Frenkel pair defects [1]. This disordered structure is characterized by an absence of translational periodicity that is accompanied by a continuous spectrum of locally defined structures [2,3]. This lack of crystalline structure in amorphous alloys may (or may not) provide substantial advantages in terms of radiation resistance. In terms of material properties, metallic glasses exhibit acceptable toughness [4–8], high strength [9–13], exceptional hardness [14–16], wear and corrosion resistance [17–21]. Additionally, BMGs have exhibited room temperature irradiation resistance [1,22]. One perceived disadvantage is that these alloys do not work harden like crystalline alloys, and exhibit deformation in the form of localized shear bands [3,5,23]. It is interesting to note that although the percent strain within a shear band is quite large, it does little to contribute to the overall plastic strain [24].

Therefore, it has been suggested that bulk metallic glasses could potentially be a viable material for use in different components of advanced fission or fusion reactors such as piping or windows. Table 1 shows previous studies which investigated the effects of neutron irradiation on amorphous alloys [25–30]. For these experiments, samples were irradiated by neutrons at various energies and temperatures that ranged from ambient to ~120 °C. As can be observed in the table, none of the metallic glasses were found to crystallize during irradiation.

In terms of the mechanical properties, a couple of investigations reported that neutron irradiation led to an embrittlement of the alloy [25–27]. For instance, Gupta et al. observed that helium formation was a possible cause of embrittlement in $Fe_{40}Ni_{40}B_{20}$

* Corresponding author. University of Tennessee, Knoxville, TN, 37996, USA.
** Corresponding author. University of Tennessee, Knoxville, TN, 37996, USA.
E-mail addresses: brechtljm@ornl.gov (J. Brechtl), szinkle@utk.edu (S.J. Zinkle).

https://doi.org/10.1016/j.jnucmat.2019.151771
0022-3115/

Table 1
Summary of neutron irradiation studies in amorphous alloys. R.T.: Room temperature.

Alloy	Specimen Type	Neutron Energy	Neutron Fluence (cm^{-2})	Irr. Temp (°C)	Crystallized? (Y/N)	Source
$Fe_{40}Ni_{40}B_{20}$	Ribbon	Thermal	10^{18}–10^{19}	~R.T.	N	[25]
$Fe_{78}Si_9B_{13}$	Ribbon	Thermal	10^{18}–10^{19}	~R.T.	N	[25]
$Fe_{40}Ni_{40}B_{20}$	Ribbon	Thermal, fast	8×10^{19}	<70	N	[26]
$Fe_{40}Ni_{40}B_{20}$	Ribbon	Thermal, fast	6.5×10^{19} (thermal) 4.3×10^{19} (fast)	<120	N	[27]
$(Mo_{0.6}Ru_{0.4})_{82}B_{18}$	Foil	1 MeV	1×10^{19}	R.T.	N	[28]
Ni_xP_{1-x} $0.15 < x < 0.26$	Electroplate	15 meV	5.91×10^{10}	–	N	[29]
$Fe_{73.5}Cu_1Nb_3Si_{13.5}B_9$	Ribbon	Thermal	3×10^{17}-10^{19}	<70	N	[30]

metallic glass, and not phase separation or cluster formation [25]. However, this result is not surprising since approximately 20% of the initial boron transmutes into He during neutron irradiation [31–33]. Gerling et al. [26] reported that the cause of embrittlement in the $Fe_{40}Ni_{40}B_{20}$ metallic glass was attributed to phase separation or $(Fe, Ni)_3B$ cluster formation that results from radiation enhanced diffusion. Furthermore, transmission electron microscopy results showed that this alloy could remain amorphous after calculated neutron doses of ~26 dpa near room temperature (where most of the displacement damage was due to B transmutation recoils) [27]. It has also been suggested that embrittlement may be the result of the structural relaxation of the alloy induced by the thermal annihilation of excess free volume in the glass [34].

On the other hand, some studies have also reported that neutron irradiation led to an increase or restoration in the ductility of metallic glass [28,30,35]. For example, a study conducted by I. Skorvanek et al. found that the ductility of thermally embrittled $Fe_{73.5}Cu_1Nb_3Si_{13.5}B_9$ amorphous ribbons could be restored by neutron irradiation [30]. In Ref. [34], the restoration of ductility in $Fe_{40}Ni_{40}B_{20}$ metallic glass was attributed to a generation of excess free volume or swelling during irradiation. They concluded that the observed swelling resulted from the creation of radiation induced defect zones, and not by any changes in composition during irradiation.

The effects of neutron irradiation on the microstructure in amorphous alloys has also been the subject of previous research. One study involved the irradiation of $Fe_{78-x}Ni_xSi_8B_{14}$ (with $x = 0, 15, 25, 38, 53, 58$) amorphous ribbons with thermal neutrons to a fluence of 10^{19} n/cm^2 [36]. Mössbauer spectroscopy revealed that before irradiation, increasing the Ni concentration in (Fe, Ni)-metalloid glass drove Fe atoms to sites with higher metalloid nearest coordination. Furthermore, it was found that neutron irradiation tended to randomize the system, partially destroying the occupancy of metalloid depleted sites by Ni.

Despite the previously mentioned research on the irradiation of metallic glasses, there are currently no known prior studies on the effects of neutron irradiation ($E > 0.1$ MeV) on Zr based BMGs. Furthermore, there are no studies which have compared the effects of irradiation damage and heat treatment on the nanoscale mechanical properties of amorphous alloys. The current investigation examines the effects of neutron irradiation and annealing on the nanoindentation hardness and short-range ordering of a Zr-base BMG alloy. This work expands upon previous studies that examined the competing effects of irradiation and annealing on the properties of metallic glasses. Therefore, the present endeavor is intended to increase the knowledge pertaining to the effects of annealing and irradiation displacement damage on the behavior of these complex alloy systems.

2. Experimental procedures

The $Zr_{52.5}Cu_{17.9}Ni_{14.6}Al_{10}Ti_5$ (BAM-11) BMG alloy was fabricated at ORNL by arc melting in an argon atmosphere using a mixture of base metals with the following purities: 99.5% Zr, 99.99% Cu, 99.99% Ni, 99.99% Al, and 99.99% Ti. As was done in Ref. [37], the alloys were then remelted and drop cast in a Zr-gettered helium atmosphere. Subsequently, the rod was remelted and drop cast into a water-cooled 7 mm diameter cylindrical Cu mold contained within a Zr-gettered helium atmosphere. Differential scanning calorimetry and X-ray Diffraction (XRD) characterization of the drop cast rod confirmed the material to be fully amorphous. After the microstructural confirmation, the samples were prepared from the as-cast rods by an electrical discharge machine.

After fabrication, BAM-11 BMG specimens were exposed to neutron irradiation at the ORNL High Flux Isotope Reactor. Here the samples were exposed to a neutron fluence of 1.4×10^{20} n/cm^2 ($E > 0.1$ MeV), which corresponded to a damage level of ~0.1 displacements per atom (dpa), in a perforated hydraulic rabbit capsule. To keep the samples at an average temperature of ~70 °C during irradiation, specimens were wrapped in aluminum foil such that the external surface of the foil was directly exposed to flowing primary loop water coolant. To compare the effects of thermal annealing, some as-cast and irradiated samples were annealed at 325 °C for 72 h and 300 °C for two weeks. The samples were heated using a ramp rate of ~5 °C/min under vacuum (~10^{-6} torr) and then cooled at a rate of ~5 °C/min after annealing.

Microstructural characterizations of the irradiated and annealed bulk metallic glass specimens were performed via neutron diffraction at the Spallation Neutron Source at Oak Ridge National Laboratory. For the neutron diffraction experiments, samples were carefully suspended in 6 mm diameter vanadium cups in which glass wool was centered on top of the canister. Samples were positioned such that their cross-sectional area was perpendicular to the neutron beam. Here, samples with a mass of ~0.5 g were exposed to a neutron flux of ~10^8 n/cm^{2}s and environmental temperature of 25 °C for a duration of 3 h. After data was collected, PDFgetN software was utilized to determine the pair distribution function (PDF).

The TEM characterization was conducted in the Low Activation Materials Development and Analysis (LAMDA) laboratory at ORNL and the Joint Institute for Advanced Materials (JIAM) at the University of Tennessee. The electron transparent TEM foils were fabricated using an FEI Quanta Dual-beam focused ion beam (FIB)/SEM with a final thinning step of 2 kV Ga + ions at a glancing angle of about 4° to minimize ion beam milling damage. After the thinning step, the sample was polished using a Fischione Nanomill 4 keV Ar + ion polisher at low incident angles. The unirradiated and irradiated samples were then examined in the ZEISS LIBRA 200 HT FE (at JIAM) and JEOL JEM-2100F TEM/STEM (at LAMDA), respectively. The TEM bright field (BF) images and diffraction patterns (DPs) were all taken using an acceleration voltage of 200 kV.

To examine the effects of neutron irradiation and annealing on the volume of the alloy, density measurements were performed at room temperature. This was done using an immersion density instrument, which consists of an ultra-sensitive balance, the Satorius ME215S, a density kit, and a high-precision digital thermometer.

Samples were immersed in a 3 M FluorinertTM Liquid FC-43 which has high density, low surface tension, low thermal expansion, low vapor pressure and low water/air solubility. At least five measurements were taken for each sample condition.

Nanoindentation experiments were performed at room temperature using a KLA-Tencor G200 Nano-indenter with a Berkovich diamond (3-sided pyramidal tip) in continuous stiffness measurement mode with a constant loading rate of 400 μNs^{-1}. For statistical accuracy, ~20 indents were made where the contact stiffness was measured as a function of depth from the point of contact of the nanoindenter with the surface to a depth of ~2,500 nm. From the stiffness measurements, the nanoindentation hardness and Young's modulus were estimated. In terms of these values, data below a depth of ~100 nm and ~200 nm, respectively, were omitted from the specimen surface due to large data scatter and anomalously high values that are associated with surface roughness. Hardness was calculated using the Oliver and Pharr method [38,39]. The area function of the tip in addition to the machine stiffness for the nanoindenter was calibrated by indenting on a standard fused silica sample [1].

Bulk hardness measurements were performed at room temperature using a Buehler Micromet 3 hardness indenter equipped with a Vickers indenter tip. The tests were performed on the as-cast, neutron irradiated (0.1 dpa) and the unirradiated annealed sample (300 °C, 2 weeks). For each indent, a 500 gf load with a dwell time of 15 s was used. Five indents were taken on each specimen to a depth of ~6.5 μm and spaced 500 μm apart. Prior to indentation, both specimens were surface polished with 1 μm diamond lapping film.

The 3-point bending tests were performed using a MTS model Insight 2−52 tensile screw-driven machine with a load capacity of 2 kN. Specimens consisted of rectangular coupons with linear dimensions of $3 \times 5 \times 0.9\ mm^3$. Before testing, samples were mechanically polished to a mirror finish using colloidal silica. During the experiment, a computer interface system which utilizes MTS TestSuite™ TW Software was used to record the load vs. crosshead displacement data for an applied crosshead speed of 0.1 mm/s.

To examine the effects of annealing on the microstructure of the BAM-11 BMG during compression, in-situ high energy XRD was conducted on the as-cast and the unirradiated annealed sample (300 °C, 2 weeks) via synchrotron XRD at the 1-ID beam line of the Advanced Photon Source at Argonne National Laboratory. Samples were cut into rectangular geometries with dimensions of $4 \times 2 \times 1.5\ mm^3$. In-situ high-energy XRD during mechanical deformation was performed on the samples exposed to a maximum compressive stress of 1.5 GPa. The beam energy at 1-ID was 100 keV ($\lambda = 0.12358$ Å). 2D detectors with 2048×2048 pixels and 200 μm × 200 μm pixel size were used to collect data. The detector was placed about 40 cm behind the sample. Calibration was performed using the CeO_2 NIST powder standard. The high-energy X-ray 2D diffraction data were processed by FIT2D software [40] to correct the data. Because of the elastic deformation induced anisotropy [41], anisotropic PDF analysis was applied [42]. For this analysis, the spherical harmonic expansion and Bessel transformation were applied to the data in which the isotropic and anisotropic PDFs were generated and analyzed.

3. Results

Fig. 1(a)-(e) displays the TEM BF and DPs of the as-cast, neutron irradiated (0.1 dpa), and the unirradiated annealed specimens. The BF imaging did not reveal the presence of any nanocrystallites in any of the samples, indicating that the samples remained amorphous during irradiation and annealing at the prescribed temperatures and neutron dose. This lack of crystallization was further confirmed by the corresponding DP, where there were only concentric rings with no observable Bragg spots or rings in the pattern.

Fig. 2 shows the PDFs obtained from the neutron diffraction of the as-cast, un-irradiated annealed, and neutron irradiated (annealed and non-annealed) BAM-11 BMG samples in which the inset highlights the upper portion of the first peak. The wavy pattern of the PDFs signifies the amorphous nature of the samples, indicating that they did not crystallize during neutron irradiation or annealing. Furthermore, the changes in the profile of the peaks suggest that the microstructure of the metallic glass underwent changes caused by both primary knock-on events and thermal treatment. For instance, the non-irradiated sample annealed at 300 °C for two weeks had the highest and most narrow (smallest FWHM) peak as compared to the other conditions. In contrast, the specimen that underwent irradiation without heat-treatment exhibited the opposite trend. On the other hand, the samples that underwent post-irradiation annealing exhibited peak behavior that was intermediate between the as-received and the irradiated-only cases. In particular, the sample heated at 325 °C for 72 h after irradiation had a slightly larger peak as compared to 0.1 dpa annealed at 300 °C for two weeks.

Table 2 displays the results of the immersion density

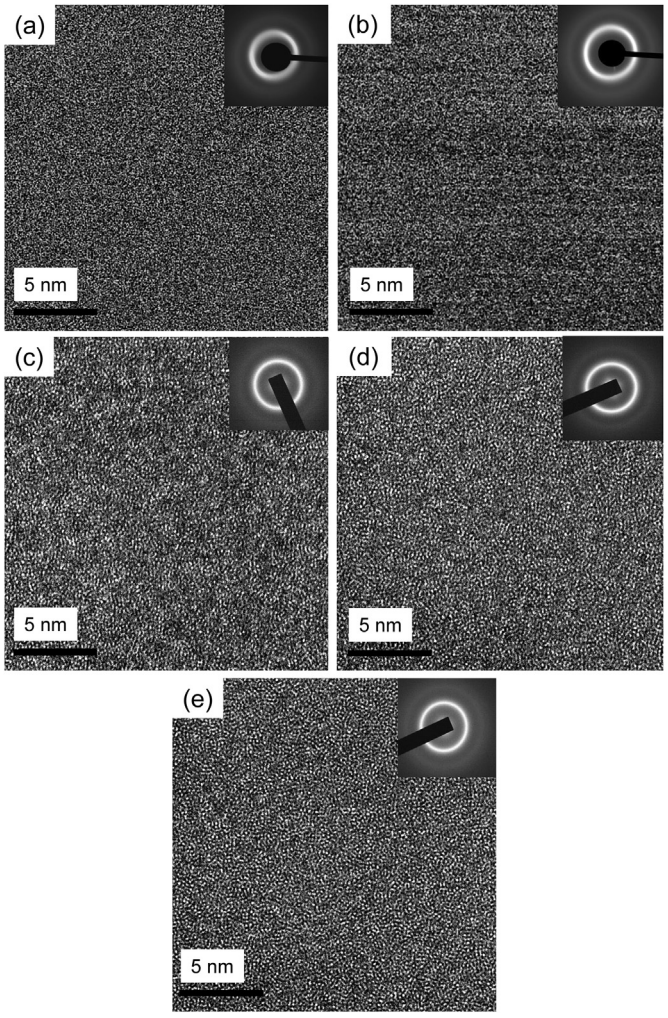

Fig. 1. TEM SAD and BF images for the (a) as-cast, (b) annealed 300 °C (2 weeks), (c) neutron irradiated (0.1 dpa), (d) neutron irradiated (0.1 dpa) and post-annealed 325 °C (72 h), and (e) neutron irradiated (0.1 dpa) and post-annealed 300 °C (two weeks).

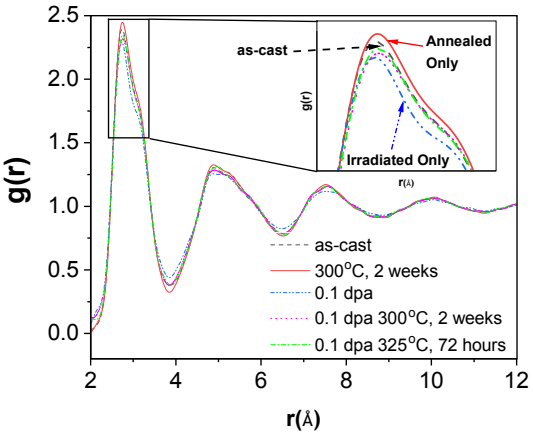

Fig. 2. The pair distribution function for the neutron irradiated and annealed BAM-11 BMG.

measurements. The density of the irradiated-only specimen was the lowest as compared to all other conditions, with a value ~2% below the as-cast density. In contrast, the density was highest for the unirradiated as-cast sample heated at 300 °C for two weeks, with a value ~1% higher than the as-cast density. Thermal annealing of the neutron irradiated samples restored the density to within ~0.5% of the as-cast state density; the samples heat treated after irradiation had density values that were in between the purely irradiated and the as-cast condition.

To examine how annealing and irradiation affects the disordered structure in the alloy, the first coordination number (CN) was estimated from the pair distribution function curves (Fig. 2) using Eq. (1):

$$C.N._i = 4\pi\rho \int_{r_{i-1}}^{r_i} r^2 g(r) dr \quad (1)$$

where g(r) is the PDF, ρ is the calculated number density of the BAM-11 BMG for the different conditions (using values listed from Table 2). The CN is important since it is linked to the degree of structural disorder in the metallic glass [43]. The calculated values for the first CN are displayed in Table 3. Interestingly, this behavior exhibited a similar trend as compared to the density and the neutron diffraction results. Namely, the neutron irradiation without heat treatment led to a decrease in CN as compared to the as-received condition while annealing without irradiation had the opposite effect. Furthermore, the coordination numbers for the samples heat treated after irradiation were greater than the one for the irradiated only sample. Moreover, the coordination number for the sample annealed at 300 °C for two weeks after irradiation was larger than the sample post-annealed at 325 °C for 72 h. Fig. 3 shows the plot of the immersion density vs. the first CN. As can be observed, there was a strong linear coorelation between the

Table 2
Immersion density measurements for the as-cast, neutron irradiated, and annealed BAM-11 BMG.

Sample Condition	Density (g/cm^3)
As-cast	6.67 ± 0.02
Annealed 300 °C 2 weeks	6.73 ± 0.02
0.1 dpa	6.53 ± 0.02
0.1 dpa 300 °C 2 weeks post-anneal	6.64 ± 0.02
0.1 dpa 325 °C 72 h post-anneal	6.63 ± 0.01

Table 3
First coordination numbers for the irradiated, as-cast, and annealed BAM-11 BMG.

Sample Condition	1st C. N.
As-cast	12.86
Annealed 300 °C 2 weeks	13.07
0.1 dpa	12.24
0.1 dpa 300 °C 2 weeks post-anneal	12.67
0.1 dpa 325 °C 72 h post-anneal	12.64

macroscopic density and the coordination number (R^2 value was 0.99).

Fig. 4 presents the nanoindentation hardness vs. depth results for the five experimental conditions discussed above. The measured hardness decreased with respect to the nanoindentation depth for all conditions (indentation size effect). Importantly, neutron irradiation to a dose of 0.1 dpa was found to significantly decrease the hardness at a given depth as compared to the as-received state. Similar to the observed trends for the neutron diffraction and immersion density results, annealing to 300 °C for two weeks had the opposite effect of inducing an increased hardness as compared to the as-cast condition. Moreover, heating after irradiation negated some of the softening induced by irradiation. Interestingly, post-irradiation annealing at 300 °C for two weeks and 325°C for 72 h produced similar changes in the hardness following irradiation. Vickers hardness values of the as-cast, neutron irradiated, and unirradiated annealed (300 °C, 2 weeks) BAM-11 BMG specimens are presented in Table 4. For the neutron irradiated sample (0.1 dpa, ~70 °C), there was a modest hardness increase of ~7%. On the other hand, the hardness significantly increased (25%) after annealing at 300 °C.

The bulk hardness was also evaluated from the nanoindentation data using the Nix-Gao extrapolation technique [44]. The results of the analysis are displayed in Table 5, and as can be seen, the extrapolated hardness values followed a similar trend as the neutron diffraction and density results. In contrast to the slight hardening observed for the bulk Vickers hardness tests, it was found that the neutron irradiation led to a −47% change in the extrapolated (from nanoindentation testing) bulk hardness value as compared to the as-cast condition. For the 300 °C, 2 weeks annealed condition of the as-cast sample, however, there was a 15% increase in the extrapolated bulk hardness value as compared to the as-cast condition; this followed a similar trend as the thermal annealing result from the Vickers hardness tests. It should be

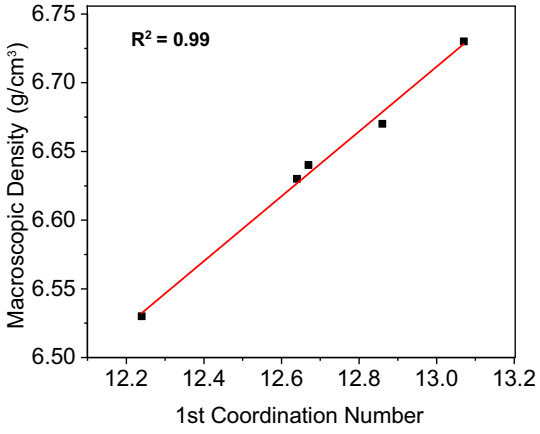

Fig. 3. The immersion density vs. the first coordination number for the as-cast, neutron irradiated, and annealed BAM-11 BMG.

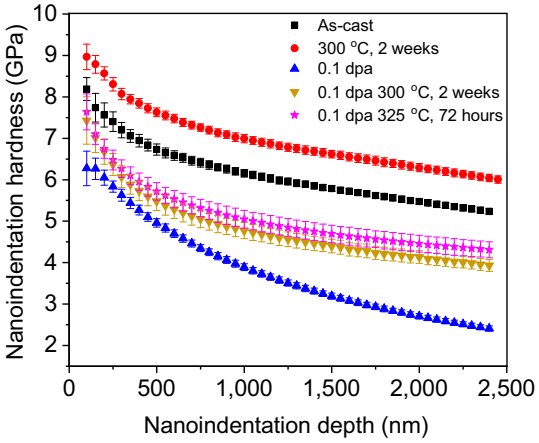

Fig. 4. The nanoindentation hardness vs. nanoindentation depth for the as-cast, neutron irradiated, and annealed BAM-11 BMG.

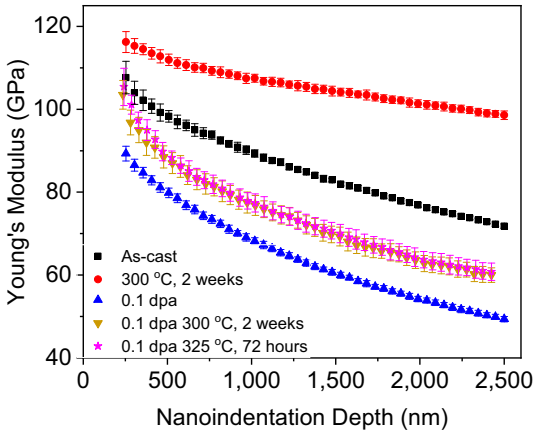

Fig. 5. The nanoindentation Young's modulus vs. nanoindentation depth for the as-cast, neutron irradiated, and annealed BAM-11 BMG.

Table 4
Vickers hardness results for the as-cast, neutron irradiated (0.1 dpa), and unirradiated annealed samples (300 °C, 2 weeks) BAM-11 BMG.

Sample Condition	Hv
As-cast	444.7 ± 5.2
0.1 dpa	474.9 ± 27.8
Annealed 300 °C, 2 weeks	560.0 ± 6.4

Table 5
Nix-Gao extrapolated hardness results for the as-cast, neutron irradiated, and annealed BAM-11 BMG samples.

Sample Condition	Nix-Gao Extrapolated Hardness (GPa)
As-cast	5.58
Annealed 300 °C 2 weeks	6.41
0.1 dpa	2.97
0.1 dpa 300 °C 2 weeks post-anneal	4.11
0.1 dpa 325 °C 72 h post-anneal	4.44

mentioned that the nanoindentation hardness data did not obey the linear trend for the square of the measured nanoindentation hardness versus the reciprocal of indentation depth that is predicted by the Nix-Gao extrapolation model. This discrepancy suggests that the Nix-Gao model, which was developed for crystalline materials, may not be applicable to metallic glasses. A similar deviation away from linearity in the Nix-Gao analysis was also observed for as-cast and ion irradiated (9 MeV Ni^{3+}) BAM-11 BMG specimens [22].

The nanoindentation Young's modulus vs. depth results for the five experimental conditions are displayed in Fig. 5. Similar to the hardness results, the measured modulus decreased with respect to the nanoindentation depth for all of the conditions. Furthermore, as compared to the as-cast state, neutron irradiation (0.1 dpa) led to a significant decrease in the modulus for all depths. Also, annealing at 300 °C for two weeks had the opposite effect of inducing an increased modulus compared to the as-cast condition. It was also observed that annealing after irradiation led to values that were intermediate between the irradiated (without annealing) and the as-cast samples.

Fig. 6 presents the flexural stress-displacement (deflection) curves for the neutron irradiated and annealed BAM-11 BMG. The corresponding strain is also plotted as a secondary abscissa on the graph. All specimens fractured with very limited plastic tensile elongation (<0.5%). The as-cast sample exhibited slight deformation (~0.5%) before fracturing. The flexural data for the unirradiated annealed sample (300 °C, 2 weeks) is not shown since the specimen fractured during initial loading after approximately 10 N (0.4 MPa) was applied during the test. As compared to the other samples, the specimen that was annealed at 325 °C for 72 h after being irradiated to a dose of 0.1 dpa reached the largest stress before fracturing, namely ~3.3 GPa. Similar to the trend displayed in the nanoindentation data (Figs. 4 and 5), the linear gradient of the curves for the samples that were annealed after irradiation displayed behavior that were intermediate between that of the as-cast and irradiated only conditions. Compared to the dynamic Young's modulus measurements for the as-cast and neutron irradiated samples (75–79 GPa) in the previous work [45], the modulus values calculated from the elastic loading portion of the flexure curves are much lower; the observed slopes are likely only measuring the stiffness of the test machine and fixture since precise specimen extensometry was not used for these tests.

Fig. 7(a)-(b) compares the high-energy XRD results for the isotropic PDF, $\rho_0^0(r)$, of the uncompressed BAM-11 BMG (as-cast and annealed) specimens. As can be observed in Fig. 7(a), the general shape of the curves are quite similar. However, the first peak for the annealed specimen annealed at 300 °C (2 weeks) exhibited a greater amplitude, which is clearly evident in Fig. 7 (b). As can be seen in the inset in Fig. 7 (b), the first peak of the $\rho_0^0(r)$ for the

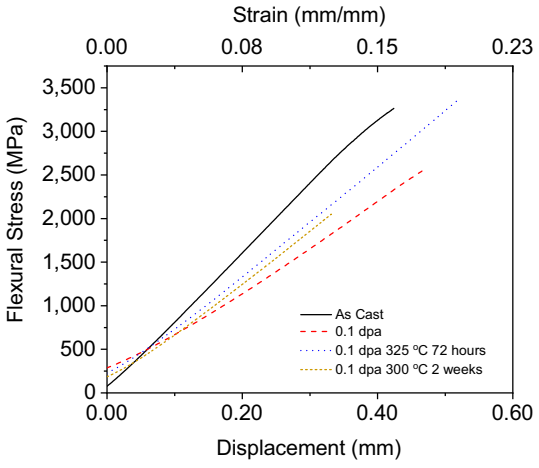

Fig. 6. Flexural stress–displacement (deflection) curve for the neutron irradiated and annealed BAM-11 BMG.

annealed sample exhibits a slightly higher and narrower profile as compared to the as-cast condition. This result indicates that annealing led to structural relaxation in the BMG which is accompanied by a more ordered microstructure.

The anisotropic component of the PDF, ρ_2^0 (r), for the as-cast and annealed (300 °C, 2 weeks) specimens that were subjected to an applied stresse of 1.5 GPa, is displayed in Fig. 8(a)-(b). Here, ρ_2^0 (r) was calculated using a spherical Bessel transformation as described in Ref. [41]. At the long r range, beyond 8 Å, the anisotropic PDF of the as-cast and annealed specimen overlap with each other. However, below 8 Å, especially in the first shell range (Fig. 8 (b)), the amplitude of ρ_2^0 (r) for the as-cast specimen is smaller than that of the annealed specimen.

To further interpret the anisotropic PDF results, a reference state of the sample under affine deformation is introduced [46], namely the affine anisotropic PDF, $\rho^0_{2,\,aff}$(r), which corresponds to the ideal elastic (affine) deformation of the sample. Fig. 9 displays the fitting of the affine anisotropic PDF to the experimental anisotropic PDF, i.e., $\rho^0_{2,\,aff}(r)$ to $\rho^0_{2,\,exp}(r)$ of the as-cast BAM-11 BMG sample. As can be observed in the inset that is located in the bottom right side of Fig. 9, there is a sufficiently good fit for r > 6.5 Å. However, there is a clear difference at small distances (see inset in top half of Fig. 9), especially in the first nearest neighbor shell, suggesting that local structural relaxation during mechanical deformation is activated by the stress exerted on the specimen. Fig. 10 displays the deviation of

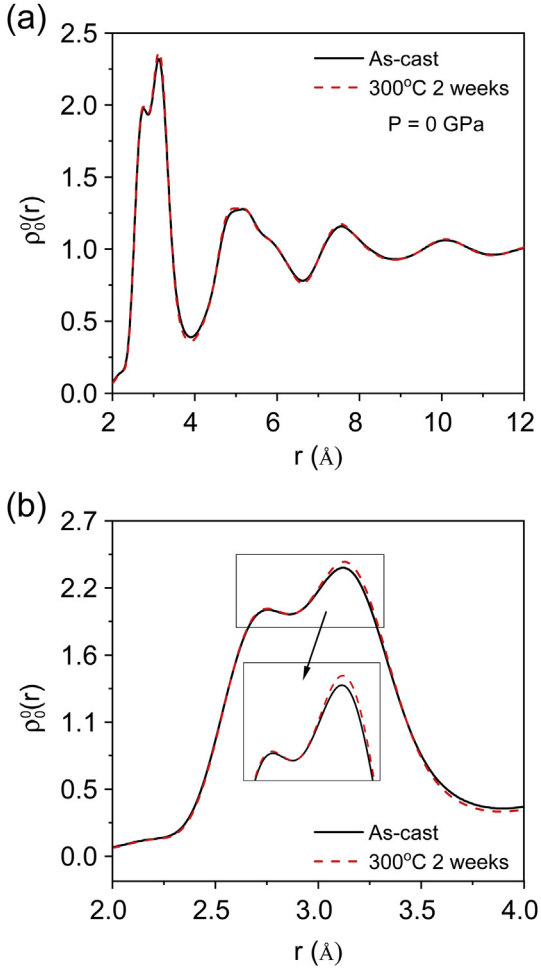

Fig. 7. (a) Comparison of the isotropic PDF, ρ_0^0 (r) and a (b) comparison of the first peak in the isotropic pair distribution function, $\rho_0^0(r)$, for the as-cast and the unirradiated annealed (300 °C 2 weeks) BAM-11 BMG samples that were uncompressed.

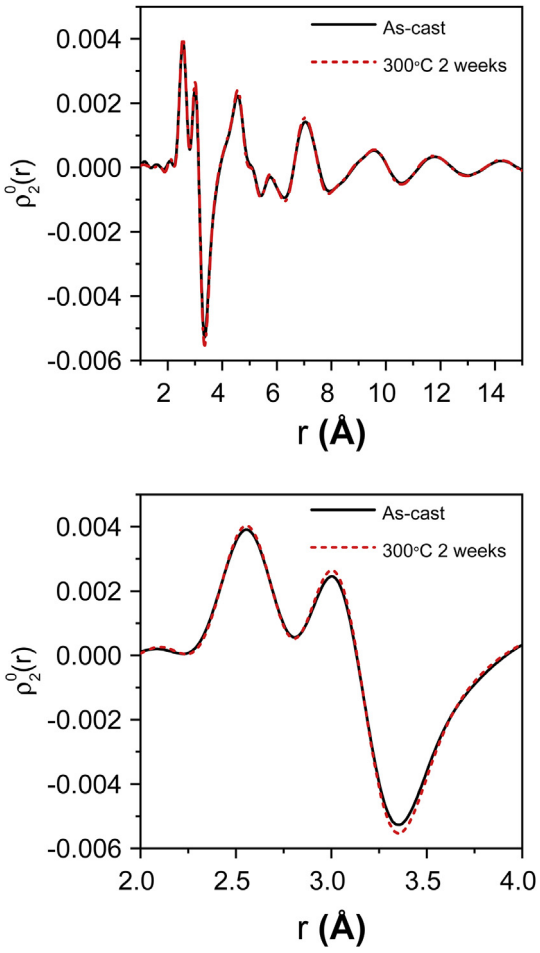

Fig. 8. Comparison of the anisotropic PDF, ρ_2^0 (r), for the as-cast and the unirradiated annealed (300 °C 2 weeks) BAM-11 BMG samples compressed at a stresse of 1.5 GPa.

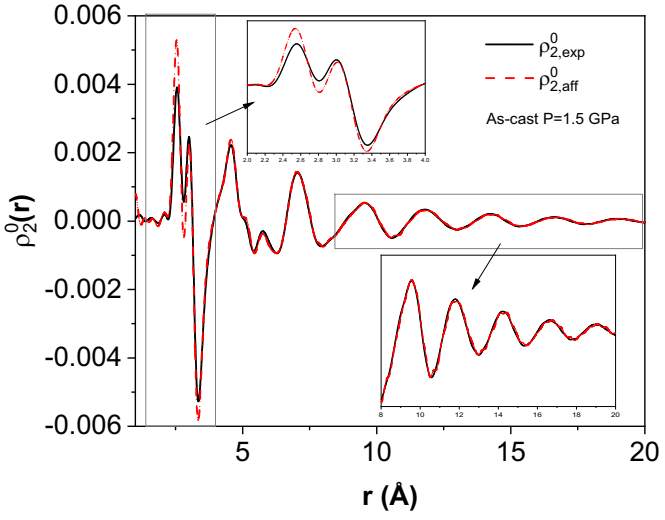

Fig. 9. The anisotropic PDF, $\rho^0_{2,exp}(r)$, of the as-cast BAM-11 BMG sample subjected to the stress of 1.5 GPa (solid black line), compared to the anisotropic PDF of the sample under affine deformation (red dashed line) for the as-cast condition. As observed in the inset, the fit is very good beyond ~6.5 Å, however, noticeable differences can be observed at smaller distances.

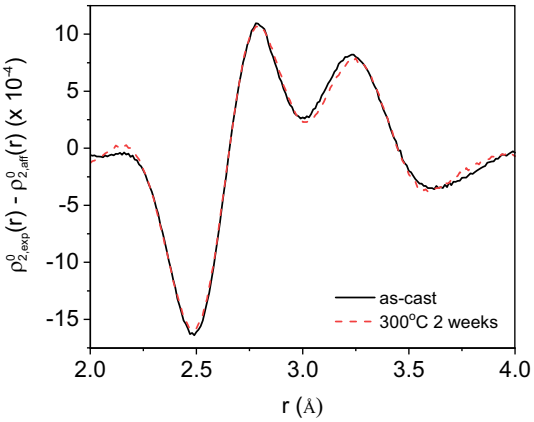

Fig. 10. The difference $\rho^0_{2,exp} - \rho^0_{2,aff}$ for the as-cast and the unirradiated annealed (300°C, 2 weeks) BAM-11 BMG samples.

the experimental anisotropic PDFs from the affine anisotropic PDF, $\Delta\rho^0_2 = \rho^0_{2,exp} - \rho^0_{2,aff}$ for both the as-cast and annealed conditions. It is found that in the first shell, the annealed sample exhibited a smaller amplitude in the oscillations as compared to the as-cast specimen. This result indicates that the BAM-11 BMG underwent structural relaxation during annealing and is therefore less susceptible to relaxation under an applied load as compared to the as-cast sample. Furthermore, this decreased susceptibility is accompanied by an embrittlement of the glass.

4. Discussion

As observed in Fig. 2, the PDF curve for the sample irradiated to 0.1 dpa had a slightly lower and broader peak as compared to the as-cast condition, indicating that neutron collision cascades led to slight structural disordering (rejuvenation) in the alloy. On the other hand, annealing BAM-11 BMG at 300 °C for 2 weeks resulted in a taller and narrower peak, which is evidence for an increase in the short-range order (relaxation). It should be emphasized that this structural relaxation was not a result of the crystallization of the specimens during heating, as indicated by the TEM results [see Fig. 1(a)–(e)]. This result was also observed in the synchrotron diffraction results, where peak narrowing (and heightening) occurred in the annealed specimen [see Fig. 7(a)–(b)]. Thus, it can be surmised from the above results that neutron irradiation leads to slight structural rejuvenation in BAM-11 BMG. Interestingly, annealing the BMG after neutron bombardment was found to partially reverse the structural disordering in the glass, as exhibited by a narrower and increased peak height. Furthermore, annealing at 325 °C for 72 h appears to have a slightly greater reversing effect as compared to heating at 300 °C for 2 weeks, as illustrated by a relatively higher peak.

Furthermore, the neutron diffraction results are apparently correlated with the macroscopic density data, as can be surmised from Tables 2 and 3 and Fig. 3. As previously discussed, neutron irradiation led to a decrease in the density of the glass. Since a decrease in the density of a metallic glass corresponds to an increase in the free volume of the alloy, an increase in the free volume content during neutron irradiation is therefore accompanied by atomic disordering. This correlation is observed for the first nearest neighbor shell. Thus, it appears that the irradiation induced rejuvenation in the alloy corresponds to a decrease in the density that is associated with the introduction of free volume/anti-free volume defects [47,48]. This increase in the free volume content of a Zr based metallic glass after neutron irradiation was reported by Yang et al. [49]. The irradiation induced structural disordering also appears to correspond to a decrease in the coordination number in the alloys, which also supports the theory that irradiation induced disordering is tied to the creation of free volume in the matrix. In contrast, annealing the alloy, which corresponds to structural relaxation, leads to an increase in the macroscopic density and the coordination number.

The nanoindentation results and three-point bend test results, as shown in Figs. 4–6, follow a similar trend as the neutron diffraction and immersion density measurements. Namely, the irradiation induced disordering leads to softening and a decreased modulus in the metallic glass, while heating results in hardening and an increased modulus. However, this softening was not clearly observed in the Vickers hardness results, which was unexpected since the bulk Vickers hardness should have a similar trend as the nanoindentation hardness behavior. With respect to the annealed only sample, the depth dependent nanoindentation hardness behavior followed a similar trend as the Vickers microhardness testing, where both tests yielded significant hardening in the alloy after annealing compared to the as-cast condition.

The discrepancies between the extrapolated hardness (Nix-Gao) and the Vickers hardness values (see Tables 4 and 5) may be a consequence of a surface modification which affects the strain gradient plasticity of the BAM-11 BMG. In addition, the nanoindentation hardness data did not obey the linear trend between the square of the measured hardness and the inverse indentation depth that is predicted by the Nix-Gao model. This deviation of the data might be associated with the amorphous structure of the BAM-11 BMG, i.e., it does not contain dislocations that are required by the model [44]. This nonlinearity of the data was previously observed in BAM-11 BMG nanoindentation testing after irradiation by 9 MeV Ni^{3+} ions to a midrange dose of 10 dpa [22].

Based on the neutron PDF results (see Fig. 2), the softening exhibited by the alloy after neutron irradiation is accompanied by an increase in the atomic disordering (and free volume), and hence rejuvenation that is induced by primary knock-on events. Pan et al. observed that rejuvenation of a metallic glass via mechanical deformation led to a decrease in the microhardness in $Zr_{64.13}Cu_{15.75}Ni_{10.12}Al_{10}$ BMG [50]. Furthermore, they suggested that rejuvenation in a metallic glass also reduces the yield stress. Since the results suggest that the free volume content is inversely related to the density, it appears that introducing regions of lower density into the specimen corresponds to a decreased resistance to yielding. Furthermore, it is suggested that this decrease in the hardness may be linked to the creation of soft-zone defects, as discussed in Ref. [51]. On the other hand, the increase in hardness is most likely due to the thermally induced structural relaxation occurring in the alloy [52]. The link between free volume and hardness was also discussed in Ref. [53], where they proposed that a decrease in free volume, which accompanies structural relaxation, results in a higher resistance to plastic deformation.

The increase in the modulus during annealing may be due to the thermal annihilation of soft-zone defects during structural relaxation. It has been proposed that soft-zone defects, which can be thought of as liquid-like atoms and their neighbors [54,55], consist of structural heterogeneities [56] that can accommodate shear deformation under an applied load. Thus, these defects can be thought of as loosely packed regions that are less resistive during an applied stress. Egami et al. showed that an increase in the number of liquid-like sites in the glassy matrix results from a change in the distribution of atomic level stresses and volume in a metallic glass [57,58]. Thus, it can be thought that neutron irradiation leads to the creation of these defects. On the other hand, Li et al. [51,59] found that annealing reduces the concentration of these defects in the glass, which in turn leads to embrittlement of the alloy. This

suggestion is supported by the results of the high energy XRD, where the difference in the anisotropic PDFs was more pronounced for the as-cast, as compared to the annealed sample (Fig. 10).

Since these soft-zone defects consist of free volume, and hence are lower in density, their destruction would lead to a decrease in the local interatomic distance throughout the glass. Furthermore, since the modulus is inversely proportional to the distance between neighboring atoms, a decrease in the quantity of these defects, therefore, would lead to an increase in the modulus. The thermal annealing-induced increase of the modulus in BAM-11 has also been reported in Ref. [53]. Conversely, irradiation would lead to a decrease in the modulus via the reduction in density that accompanies the creation of soft-zone defects during particle bombardment. This increase in the free volume fraction in metallic glass during irradiation was reported by Bian et al. for a Xe ion irradiated Zr based BMG [60]. Finally, the intermediate modulus values for the irradiated and annealed samples (see Fig. 5) indicates that thermal annealing reduced the number of soft-zone defects that were created during the neutron irradiation.

With regards to the high-energy XRD results, the good fitting at the long r range in Fig. 8(a) implies that the average strain at the long r range is basically affine, ε_{affine}. On the other hand, in the first nearest neighbor shell the local strain is smaller than the ε_{affine}, which results from a local structural relaxation during elastic deformation. This local relaxation is caused by the local topological rearrangement (LTR) of the BMG sample under the applied stress [41], which is characteristic of BMGs. The overlapping of the ρ_2^0 (r) at the long r range in Fig. 8(a) implies that the average strain in the as-cast and annealed BMGs during compresson is affine at the long r range. Furthermore, based on the stress-induced LTR effect that is apparent in Fig. 9, the larger amplitude of the ρ_2^0 (r) in the first shell for the annealed specimen indicates less local strain relaxation as compared to the as-cast specimen. This finding suggests that the annealed BMG is already significantly relaxed and the local LTR sites are already exhausted, resulting in the brittleness of the annealed BAM-11 BMG. This observation is reconfirmed by Fig. 10 where the difference between the $\rho_{2,\,exp}^0$(r) and $\rho_{2,\,aff}^0$(r) quantifies the local strain relaxation. More local strain relaxation (larger $\Delta\rho_2^0$) suggests a greater degree of stress accommodation during mechanical deformation, and thus an enhancement in the plasticity of the BMG. In this case, the smaller $\Delta\rho_2^0$ of the annealed specimen (Fig. 10) indicates the brittleness of the annealed BMG as compared to the as-cast sample.

Based on the above discussions, an increase in nanoindentation hardness, as observed in Fig. 4, is associated with an embrittlement in the alloy. On the other hand, neutron irradiation appears to lead to softening and a reduction in the Young's modulus which may be attributed to an enhanced ductility in the alloy. Furthermore, the hardening experienced by the BAM-11 BMG appears to correspond to a decreased ductility as observed by the nanoindentation and XRD results (Figs. 4 and 10). It was also found that the hardness of the BAM-11 BMG was higher in the samples that were annealed after irradiation as compared to the irradiated only samples.

5. Conclusions

For this study, BAM-11 bulk metallic glass was irradiated by fission neutrons to a fluence of 1.4×10^{20}/cm^2 at a temperature of ~70 °C. Neutron irradiation and thermal annealing were observed to act as competing processes with regards to their effect on the mechanical and microstructural properties of the BMG. For instance, annealing after irradiation largely reversed the atomic disordering effects caused by the irradiation. Nanoindentation hardness measurements found that irradiation led to softening and a reduction in the Young's modulus of the alloy, while annealing caused an increase in the hardness and modulus. On the other hand, Vickers hardness tests indicated that the BAM-11 BMG hardened after irradiation to a dose of 0.1, dpa. Furthermore, the sample density was reduced by ~2% after neutron irradiation but was increased by ~1% after annealing at 300 °C for two weeks. Neutron diffraction results indicated that primary knock-on events caused rejuvenation (structural disordering) while annealing resulted in structural relaxation. Additionally, synchrotron XRD linked the temperature induced structural relaxation of the alloy to a loss of ductility and increase in nanoindentation hardness, which agrees with the literature. In general, an increase in the structural disorder of the glass is linked to a softening of the alloy and perhaps also linked to a higher concentration of soft-zone defects in the alloy. Finally, results indicate that hardening caused by heat treatment corresponds to structural relaxation, densification, and a loss of ductility in the BMG, while the decrease in the ductility appears linked to the annihilation of soft-zone defects, and thus the free volume of BAM-11 BMG.

Notice

Acknowledgements

This research was sponsored by the Office of Fusion Energy Sciences, U.S. Department of Energy under contract DE-AC05-00OR22725 with UT-Battelle, LLC and grant # DE-SC0006661 with the University of Tennessee. H.W and W.D acknowledge U.S. Department of Energy, Basic Energy Sciences, Materials Science and Engineering Division. The neutron diffraction utilized ORNL's Nanoscale-Ordered Materials Diffractometer (NOMAD) at the Spallation Neutron Source (SNS) User Facility, which is sponsored by the Scientific User Facilities Division, Office of Basic Energy Sciences, U.S. Department of Energy. Synchrotron X-ray diffraction was carried out at the Advanced Photon Source, a U.S. Department of Energy (DOE) Office of Science User Facility, operated for the DOE Office of Science by Argonne National Laboratory under Contract DE-AC02-06CH11357. Finally, the authors would also like to thank Drs. Maxim Gussev and Takeshi Egami for helpful discussions regarding the nanoindentation, 3-point bend test, and neutron diffraction experiments.

Appendix A. Supplementary data

Supplementary data to this article can be found online at https://doi.org/10.1016/j.jnucmat.2019.151771.

References

[1] A.G. Perez-Bergquist, H. Bei, K.J. Leonard, Y. Zhang, S.J. Zinkle, Effects of ion irradiation on $Zr_{52.5}Cu_{17.9}Ni_{14.6}Al_{10}Ti_5$ (BAM-11) bulk metallic glass, Intermetallics 53 (2014) 62–66.
[2] Y.Q. Cheng, J. Ding, E. Ma, Local topology vs. Atomic-level stresses as a measure of disorder: correlating structural indicators for metallic glasses, Mater. Res. Lett. 1 (1) (2013) 3–12.
[3] M. Miller, P.K. Liaw, Bulk Metallic Glasses: an Overview, Springer, New York,

2008.
[4] C.T. Liu, L. Heatherly, J.A. Horton, D.S. Easton, C.A. Carmichael, J.L. Wright, J.H. Schneibel, M.H. Yoo, C.H. Chen, A. Inoue, Test environments and mechanical properties of Zr-base bulk amorphous alloys, Metall. Mater. Trans. A 29 (7) (1998) 1811–1820.
[5] S.V. Madge, Toughness of bulk metallic glasses, Metals 5 (3) (2015) 1279–1305.
[6] M.D. Demetriou, M.E. Launey, G. Garrett, J.P. Schramm, D.C. Hofmann, W.L. Johnson, R.O. Ritchie, A damage-tolerant glass, Nat. Mater. 10 (2011) 123.
[7] J. Xu, E. Ma, Damage-tolerant Zr–Cu–Al-based bulk metallic glasses with record-breaking fracture toughness, J. Mater. Res. 29 (14) (2014) 1489–1499.
[8] J.J. Lewandowski, X.J. Gu, A.S. Nouri, S.J. Poon, G.J. Shiflet, Tough Fe-based bulk metallic glasses, Appl. Phys. Lett. 92 (9) (2008), 091918.
[9] F.-F. Wu, K.C. Chan, S.-S. Jiang, S.-H. Chen, G. Wang, Bulk metallic glass composite with good tensile ductility, high strength and large elastic strain limit, Sci. Rep. 4 (2014) 5302.
[10] C.J. Gilbert, R.O. Ritchie, W.L. Johnson, Fracture Toughness and fatigue-crack propagation in a Zr-Ti-Ni-Cu-Be bulk metallic glass, Appl. Phys. Lett. 71 (1997) 476–478.
[11] Q. Wang, Y. Yang, H. Jiang, C.T. Liu, H.H. Ruan, J. Lu, Superior tensile ductility in bulk metallic glass with gradient amorphous structure, Sci. Rep. 4 (2014).
[12] X. Gu, G.J. Shiflet, F.Q. Guo, S.J. Poon, Mg-Ca-Zn bulk metallic glasses with high strength and significant ductility, J. Mater. Res. 20 (8) (2005) 1935–1938.
[13] J.M. Park, Y.C. Kim, W.T. Kim, D.H. Kim, Ti-based bulk metallic glasses with high specific strength, Mater. Trans. 45 (2) (2004) 595–598.
[14] S.V. Madge, A. Caron, R. Gralla, G. Wilde, S.K. Mishra, Novel W-based metallic glass with high hardness and wear resistance, Intermetallics 47 (2014) 6–10.
[15] M.N.M. Patnaik, R. Narasimhan, U. Ramamurty, Spherical indentation response of metallic glass, Acta Mater. 52 (11) (2004) 3335–3345.
[16] G.R. Khanolkar, M.B. Rauls, J.P. Kelly, O.A. Graeve, A.M. Hodge, V. Eliasson, Shock wave response of iron-based in situ metallic glass matrix composites, Sci. Rep. 6 (2016), 22568.
[17] A.L. Greer, K.L. Rutherford, I.M. Hutchings, Wear resistance of amorphous alloys and related materials, Int. Mater. Rev. 47 (2) (2002) 87–112.
[18] T. Xu, S. Pang, H. Li, T. Zhang, Corrosion resistant Cr-based bulk metallic glasses with high strength and hardness, J. Non-Cryst. Solids 410 (2015) 20–25.
[19] S.J. Poon, G.J. Shiflet, V. Ponnambalam, V.M. Keppens, R. Taylor, G. Petculescu, Synthesis and properties of high-manganese iron-based bulk amorphous metals as non-ferromagnetic amorphous steel alloys, Mater. Res. Soc. Symp. Proc. (2003) 167–177. Boston, Ma.
[20] W.H. Peter, R.A. Buchanan, C.T. Liu, P.K. Liaw, M.L. Morrison, J.C.A. Carmichael, J.L. Wright, Localized Corrosion behavior of a zirconium-based bulk metallic glass relative to its crystalline state, Intermetallics 10 (11–12) (2002) 1157–1162.
[21] G. Li, Y.Q. Wang, L.M. Wang, Y.P. Gao, R.J. Zhang, Z.J. Zhan, L.L. Sun, J. Zhang, W.K. Wang, Wear behavior of bulk $Zr_{41}Ti_{14}Cu_{12.5}Ni_{10}Be_{22.5}$ metallic glasses, J. Mater. Res. 17 (8) (2002) 1877–1880.
[22] J. Brechtl, S. Agarwal, M.L. Crespillo, T. Yang, H. Bei, S.J. Zinkle, Evolution of the microstructural and mechanical properties of BAM-11 bulk metallic glass during ion irradiation and annealing, J. Nucl. Mater. 523 (2019) 299–309.
[23] X. Xie, Y.-C. Lo, Y. Tong, J. Qiao, G. Wang, S. Ogata, H. Qi, K.A. Dahmen, Y. Gao, P.K. Liaw, Origin of serrated flow in bulk metallic glasses, J. Mech. Phys. Solids 124 (2019) 634–642.
[24] C.A. Schuh, T.C. Hufnagel, U. Ramamurty, Overview No.144 - mechanical behavior of amorphous alloys, Acta Mater. 55 (12) (2007) 4067–4109.
[25] A. Gupta, S. Habibi, G. Principi, Neutron irradiation effects in metallic glasses, Mater. Sci. Eng. A134 (1991) 992–995.
[26] R. Gerling, F.P. Schimansky, R. Wagner, Radiation-induced changes of the ductility of amorphous $Fe_{40}Ni_{40}B_{20}$, Scr. Metall. 17 (2) (1983) 203–208.
[27] R. Gerling, R. Wagner, Properties of in-core reactor-irradiated amorphous $Fe_{40}Ni_{40}B_{20}$, J. Nucl. Mater. 107 (1982) 311–317.
[28] E.A. Kramer, W.L. Johnson, C. Cline, The effects of neutron irradiation on a superconducting metallic glass, Appl. Phys. Lett. 35 (10) (1979) 815–818.
[29] A.K. Ibrahim, A.I.A. Aly, A. El-khatieb, T. Habib, Structural relaxations in irradiated Ni-P metallic glasses, Solid State Commun. 81 (9) (1992) 789–794.
[30] I. Skorvanek, R. Gerling, T. Graf, M. Fricke, J. Hesse, Neutron irradiation effects on the structural, magnetic and mechanical properties of amorphous and nanocrystalline $Fe_{73.5}Cu_1Nb_3Si_{13.5}B_9$, IEEE Trans. Magn. 30 (2) (1994) 548–551.
[31] M.L. Cumo, Nuclear Plants, Sapienza Università Editrice 2017.
[32] A. Bhattacharya, C.M. Parish, T. Koyanagi, C.M. Petrie, D. King, G. Hilmas, W.G. Fahrenholtz, S.J. Zinkle, Y. Katoh, Nano-scale microstructure damage by neutron irradiations in a novel Boron-11 enriched TiB_2 ultra-high temperature ceramic, Acta Mater. 165 (2019) 26–39.
[33] S.J. Zinkle, K. Farrell, H. Kanazawa, Microstructure and cavity swelling in reactor-irradiated dilute copper-boron alloy, J. Nucl. Mater. 179–181 (1991) 994–997.
[34] R. Gerling, R. Wagner, Density of neutron irradiated and annealed amorphous $Fe_{40}Ni_{40}B_{20}$, Scr. Metall. 16 (1982) 963–967.
[35] R. Gerling, F.P. Schimansky, R. Wagner, Restoration of the ductility of thermally embrittled amorphous-alloys under neutron-irradiation, Acta Metall. Mater. 35 (5) (1987) 1001–1006.
[36] A. Gupta, S. Habibi, G. Principi, Study of short range order in Fe-Ni-Si-B amorphous alloys, Mater. Sci. Eng. A304-A306 (2001) 1058–1061.
[37] A.G. Perez-Bergquist, J. Brechtl, H. Bei, Y. Zhang, S.J. Zinkle, Effects of ion irradiation on BAM-11 bulk metallic glass, in: Fusion Materials Semiannual Progress Report for Period Ending June 30, 2014 vol. 184, U.S. Department of Energy, 2014. DOE/ER- 0313/56.
[38] W.C. Oliver, G.M. Pharr, An improved technique for determining hardness and elastic modulus using load and displacement sensing indentation experiments, J. Mater. Res. 7 (6) (1992) 1564–1583.
[39] W.C. Oliver, G.M. Pharr, Measurement of hardness and elastic modulus by instrumented indentation: advances in understanding and refinements to methodology, J. Mater. Res. 19 (1) (2004) 3–20.
[40] A.P. Hammersley, S.O. Svensson, A. Thompson, H. Graafsma, A. Kvick, J.P. Moy, Calibration and correction of distortions in 2D detector systems, Rev. Sci. Instrum. 66 (1995) 2729–2733.
[41] W. Dmowski, T. Iwashita, C.-P. Chuang, J. Almer, T. Egami, Elastic heterogeneity in metallic glasses, Phys. Rev. Lett. 105 (20) (2010).
[42] T. Egami, T. Iwashita, W. Dmowski, Mechanical properties of metallic glasses, Metals 3 (2013) 77–113.
[43] J.J. Maldonis, A.D. Banadaki, S. Patala, P.M. Voyles, Short-range order structure motifs learned from an atomistic model of a $Zr_{50}Cu_{45}Al_5$ metallic glass, Acta Mater. 175 (2019) 35–45.
[44] W.D. Nix, H. Gao, Indentation size effects in crystalline materials: a law for strain gradient plasticity, J. Mech. Phys. Solics 46 (3) (1998) 411–425.
[45] J. Brechtl, N.A.P.K. Kumar, H. Bei, S.J. Zinkle, Effects of ion and neutron irradiation on BAM-11 bulk metallic glass, in: Fusion Materials Semiannual Progress Report for Period Ending June 30, 2015 vol. 223, U.S. Department of Energy, 2015. DOE/ER- 0313/58.
[46] T. Egami, Y. Tong, W. Dmowski, Deformation in metallic glasses studied by synchrotron X-ray diffraction, Metals 6 (22) (2016).
[47] T. Egami, K. Maeda, D. Srolovitz, V. Vitek, Local structure of amorphous metals, J. Phys. Colloq. 41 (C8) (1980) C8–C272. C8-275.
[48] Y. Tong, W. Dmowski, H. Bei, Y. Yokoyama, T. Egami, Mechanical rejuvenation in bulk metallic glass induced by thermo-mechanical creep, Acta Mater. 148 (2018) 384–390.
[49] L. Yang, H.Y. Li, P.W. Wang, S.Y. Wu, G.Q. Guo, B. Liao, Q.L. Guo, X.Q. Fan, P. Huang, H.B. Lou, F.M. Guo, Q.S. Zeng, T. Sun, Y. Ren, L.Y. Chen, Structural responses of metallic glasses under neutron irradiation, Sci. Rep. 7 (1) (2017), 16739.
[50] J. Pan, Y.X. Wang, Q. Guo, D. Zhang, A.L. Greer, Y. Li, Extreme rejuvenation and softening in a bulk metallic glass, Nat. Commun. 9 (1) (2018) 560.
[51] W. Li, H. Bei, Y. Tong, W. Dmowsk, Y.F. Gao, Structural heterogeneity induced plasticity in bulk metallic glasses: from well-relaxed fragile glass to metal-like behavior, Appl. Phys. Lett. 103 (2013).
[52] J. Ketkaew, M. Fan, M.D. Shattuck, C.S. O'Hern, J. Schroers, Structural relaxation kinetics defines embrittlement in metallic glases, Scr. Mater. 149 (2018) 21–25.
[53] W.H. Jiang, F.X. Liu, H. Choo, P.K. Liaw, Effect of structural relaxation on mechanical behavior of a Zr-based bulk-metallic glass, Mater. Trans. 48 (7) (2007) 1781–1784.
[54] T. Egami, Mechanical failure and glass transition in metallic glasses, J. Alloy, Compd 509 (2011) S82–S86.
[55] B. Wang, L. Luo, E. Guo, Y. Su, M. Wang, R.O. Ritchie, F. Dong, L. Wang, J. Guo, H. Fu, Nanometer-scale gradient atomic packing structure surrounding soft spots in metallic glasses, npj Comput. Mater. 4 (1) (2018) 41.
[56] W. Li, Y. Gao, H. Bei, On the correlation between microscopic structural heterogeneity and embrittlement behavior in metallic glasses, Sci. Rep. 5 (2015).
[57] T. Egami, S.J. Poon, Z. Zhang, V. Keppens, Glass transition in metallic glasses: a microscopic model of topological fluctuations in the bonding network, Phys. Rev. B 76 (2) (2007) 6.
[58] D. Srolovitz, K. Maeda, V. Vitek, T. Egami, Structural defects in amorphous solids Statistical analysis of a computer model, Philos. Mag. A 44 (4) (1981) 847–866.
[59] W. Li, Y. Gao, H. Bei, On the correlation between microscopic structural heterogeneity and embrittlement behavior in metallic glasses, Sci. Rep. 5 (2015), 14786.
[60] X.L. Bian, G. Wang, H.C. Chen, L. Yan, J.G. Wang, Q. Wang, P.F. Hu, J.L. Ren, K.C. Chan, N. Zheng, A. Teresiak, Y.L. Gao, Q.J. Zhai, J. Eckert, J. Beadsworth, K.A. Dahmen, P.K. Liaw, Manipulation of free volumes in a metallic glass through Xe-ion irradiation, Acta Mater. 106 (2016) 66–77.